Euler Equations—Implicit Schemes and Boundary Conditions

Sukumar R. Chakravarthy*
Rockwell International Science Center, Thousand Oaks, California

Implicit boundary condition procedures are presented for use with implicit finite difference schemes for the unsteady Euler equations. This new boundary point treatment is based on the mathematical theory of characteristics for hyperbolic systems of equations. Along with the theoretical background, the practical application of the method to several types of boundaries is also explained using several examples. The specific boundary conditions covered include subsonic inflow and outflow, surface tangency, and shock waves. The example problems include one-dimensional Laval nozzle flow, dual-throat rocket engine nozzle flow, and supersonic flow past a sphere. The implicit boundary treatment permits the use of large time steps allowing the finite difference algorithm to converge to the asymptotic steady state much faster than schemes that use explicitly applied boundary conditions. At least an order of magnitude increase in computational speed is demonstrated in the examples shown.

Background

THE growing popularity of solutions to the Euler equations in transonics and their continued application in supersonics have increased the need for quicker solutions. The potential of implicit schemes in this direction has not been fully exploited for want of correct, implicit application of boundary conditions. The predominant use of implicit algorithms for the Navier-Stokes equations has partly been responsible for the neglect of implicit boundary point treatment for the Euler equations. Thus, there is a need for correct and stable procedures for the easy implicit application of boundary conditions. Such methods will serve the two purposes of 1) reaching time-asymptotic steady state faster and 2) permitting a time step for truly unsteady flow that is not necessarily restricted by the CFL stability criterion but is based upon the magnitude of the transients.

For clues and information on how to construct such boundary condition procedures, one must turn to the mathematical theory of characteristics for hyperbolic systems of equations. The unsteady Euler equations belong to this category. The theory for hyperbolic systems is rich with information on signal propagation directions. The characteristics theory clearly points to the number of boundary conditions that may and need be prescribed without overdetermining the solution. Boundary condition procedures based on this theory have been known and applied for several years by Kentzer,[1] Porter and Coakley,[2] de Neef,[3] and others. In earlier work by this author,[4,5] easily understood and implementable methods for boundary point treatment were presented. However, all of the above techniques were developed for explicit finite difference schemes. It seems that it must be easy to extend such methodologies based on mathematical theory for hyperbolic systems to implicit finite difference schemes, and indeed, it is simple enough. The rest of this paper describes such implicit boundary condition procedures. The given examples illustrate in detail the application of the proposed methodology to specific types of boundaries and demonstrate the merits of the new scheme.

Presented as Paper 82-0228 at the AIAA 20th Aerospace Sciences Meeting, Orlando, Fla., Jan. 11-14, 1982; submitted Jan. 22, 1982; revision received July 26, 1982.

*Member Technical Staff; at present: Research Associate, Department of Aeronautics and Astronautics, Stanford University, Stanford, Calif. Member AIAA.

Theoretical Framework

Consider the governing quasilinear system of equations for a representative one-dimensional flow:

$$\partial_t \vec{D} + \partial_x \vec{E}(\vec{D}) + \vec{H}(\vec{D},x) = 0 \qquad t \geq 0 \qquad x_\ell \leq x \leq x_r \tag{1}$$

and its alternate representation:

$$\vec{D}_t + A(\vec{D})\vec{D}_x + \vec{H} = 0 \tag{2}$$

where t and x denote time and space, respectively; $\vec{D}$ is the m vector of dependent variables; $\vec{E}$ is the flux vector; $\vec{H}$ is a source term; and the Jacobian matrix $\partial\vec{E}/\partial\vec{D}$ is denoted by A.

Assuming that the above equations constitute a hyperbolic system, there exist real eigenvalues of the coefficient matrix A and a complete, linearly independent set of left (row) and right (column) eigenvectors.[6] Let Λ be the diagonal matrix of eigenvalues $\{\lambda_i, i=1,\ldots,m\}$ taken in order of increasing value and L be the matrix comprising the m row eigenvectors $\{\vec{\ell}_i, i=1,\ldots,m\}$ in the same order. (The $(\vec{\ })$ notation denotes both row and column vectors.) Then,

$$L(\vec{D}_t + A\vec{D}_x + \vec{H}) = 0 \tag{3a}$$

or

$$L\vec{D}_t + \Lambda L\vec{D}_x + L\vec{H} = 0 \tag{3b}$$

or

$$\vec{C}_t + \Lambda\vec{C}_x + L\vec{H} = 0 \tag{3c}$$

where,

$$\frac{\partial\vec{C}}{\partial\vec{D}} = L \tag{3d}$$

Thus, premultiplying the governing system of coupled equations (2) by the matrix of left eigenvectors results in a decoupled system of equations (3c) in new dependent variables $\vec{C}$. It is enough for our purposes to look at Eq. (3c) conceptually and it is not necessary to seek the new dependent variable $\vec{C}$ explicitly. For linear equations, $\vec{C} = L\vec{D}$, but such simplicity is strictly restricted to linear equations.

The decoupled equations (3c) may be written as

$$\partial_t c_i + \lambda_i \partial_x c_i + \vec{\ell}_i \vec{H} = 0 \qquad i = 1,\ldots,m \tag{4}$$

It is known[4] that, in a finite difference representation of each equation in Eq. (4), it is appropriate to use a backward difference approximation to $\partial_x c_i$ when the term is multiplied by positive λ_i, and forward difference approximation with negative λ_i. (For $\lambda_i = 0$, the choice of spatial discretization is arbitrary and makes no difference.) When the time discretization is implicit, such one-sided spatial discretizations can lead to unconditionally stable (for a linear model problem) schemes for each of the m equations in Eq. (4). The justification for upwind differencing based on the characteristic speeds λ_i is rigorous for linear equations and is extended to nonlinear systems by local linearization arguments. For nonlinear systems, $\vec{C}$ may not exist. In that case, Eqs. (3c) and (3d) would not be meaningful. Independent of the existence of $\vec{C}$, in each equation of Eq. (3b), it is appropriate to approximate the elements of $\vec{D}_x$ multiplied by positive λ_i by backward difference formulas, etc.

At a boundary (say at x_ℓ), some eigenvalues (negative) would imply signal propagation from the interior to the boundary point (along negative spatial direction). Others (positive) would imply information affecting the point from outside the boundary. Forward spatial discretization can correctly account for the influence of negative or zero eigenvalues. But it is incorrect to use forward finite difference formulas for the other equations. Also, grid points do not exist to the left of the boundary, thus excluding the use of backward difference formulas. Equations implying positive propagation must thus be discarded and replaced with boundary conditions. Let there be p positive eigenvalues and p boundary conditions of the type

$$B_i(\vec{D}) = 0 \qquad i = m-p+1,\ldots,m \tag{5a}$$

or its time-linear representation

$$\frac{\partial B_i}{\partial t} = \frac{\partial B_i}{\partial \vec{D}}\partial_t \vec{D} = 0 \qquad i = m-p+1,\ldots,m \tag{5b}$$

Then, the following set of equations:

$$\partial_t c_i + \lambda_i \partial_x c_i + \vec{\ell}_i \vec{H} = 0 \qquad \text{for } i = 1,\ldots,m-p$$

$$\frac{\partial B_i}{\partial \vec{D}}\partial_t \vec{D} = 0 \qquad \text{for } i = m-p+1,\ldots,m \tag{6}$$

describe the flow at the boundary point and can be solved with forward spatial discretization and implicit temporal discretization. This treatment of boundary points will result in unconditional linear stability.

Tracing backwards the steps between Eqs. (1) and (6), the last equation can be rewritten as

$$L_1 \vec{D}_t + L_2(\vec{E}_x + \vec{H}) = 0 \tag{7a}$$

or

$$\vec{D}_t + L_1^{-1} L_2(\vec{E}_x + \vec{H}) = 0 \tag{7b}$$

or

$$\vec{D}_t + L_1^{-1} L_2(A\vec{D}_x + \vec{H}) = 0 \tag{7c}$$

where

$$L_2 = \begin{bmatrix} \vec{\ell}_1 \\ \cdot \\ \cdot \\ \vec{\ell}_{m-p} \\ 0 \\ \cdot \\ \cdot \\ 0 \end{bmatrix} \begin{matrix} \text{1st row} \\ \cdot \\ \cdot \\ (m-p)\text{th row} \\ (m-p+1)\text{th row} \\ \cdot \\ \cdot \\ m\text{th row} \end{matrix} \tag{8}$$

$$L_1 = \begin{bmatrix} \vec{\ell}_1 \\ \cdot \\ \cdot \\ \vec{\ell}_{m-p} \\ \partial B_{(m-p+1)/\partial \vec{D}} \\ \cdot \\ \cdot \\ \partial B_{m/\partial \vec{D}} \end{bmatrix} \begin{matrix} \text{1st row} \\ \cdot \\ \cdot \\ (m-p)\text{th row} \\ (m-p+1)\text{th row} \\ \cdot \\ \cdot \\ m\text{th row} \end{matrix} \tag{9}$$

Thus the application of implicit boundary conditions is as simple as solving Eq. (7) at the boundary points along with Eqs. (1) or (2) at interior points using a proper implicit difference algorithm. Obviously, L_1 must be nonsingular and this condition guides the user in choosing B_i with discrimination.

So far, this paper has dealt with generalities. The remaining sections will cover particular forms of equations and boundary conditions. To conclude this section, a few obvious facts are reviewed:

1) The role of the negative and positive eigenvalues are reversed at the right boundary ($x = x_r$).

2) At boundaries, one-sided spatial difference formulas are used (forward at $x = x_\ell$ and backward at $x = x_r$).

3) L_1 will certainly be nonsingular if $\partial B_i/\partial \vec{D} = \alpha \vec{\ell}_i$, where α is a constant of proportionality. Such a choice of B_i can be used for simple, nonreflective far-field boundary conditions.

4) The number of boundary conditions required is equal to the difference between the number of unknown dependent variables and the number of characteristics that do not point from outside the domain to the boundary point.

5) The new procedure may be applied both to the conservation and nonconservation forms of the governing equations. The discrete conservation properties of the method are discussed later.

6) The boundary point equation (7) can also be used with explicit finite difference methods.

Laval Nozzle Flow

The first example, to be considered in this section, fits snugly into the mold created in the last section. The governing equation is precisely Eq. (1) with

$$\vec{D} = \begin{bmatrix} \rho \\ \rho u \\ e \end{bmatrix} \quad \vec{E} = \begin{bmatrix} \rho u \\ p + \rho u^2 \\ (e+p)u \end{bmatrix} \quad \vec{H} = \frac{A_x}{A}\begin{bmatrix} \rho u \\ \rho u^2 \\ (e+p)u \end{bmatrix} \tag{10}$$

where ρ is the density; p the pressure; the area of the Laval nozzle, $A = A(x)$; $A_x = \partial A/\partial x$; u is the velocity; $e = p/(\gamma - 1) + \rho u^2/2$; γ is the specific heat ratio.

A parabolic area distribution was used:

$$A(x) = (y_{\max} - y_{\min})x^2 + y_{\min} \qquad -1/3 \le x \le 1 \tag{11}$$

At the subsonic inflow, enthalpy, $h = \gamma p/[(\gamma - 1)\rho] + u^2/2$ and entropy, $s = p/\rho^\gamma$, were prescribed to be their stagnation chamber values. At the outflow, a constant pressure value was imposed that would result in subsonic flow there. The back pressure imposed was chosen to give risk to a shock at $x = 1/3$. To start the calculations, initially, no flow and stagnation values of pressure and density were prescribed throughout the nozzle.

The eigenvector matrix L may be shown to be

$$L=\begin{array}{|c|c|c|l|}\hline \frac{u}{\rho}+\frac{(\gamma-1)u^2}{2\rho c} & -\frac{1}{\rho}-\frac{(\gamma-1)u}{\rho c} & \frac{\gamma-1}{\rho c} & \text{row}(\lambda_1)\\ \hline 1-\frac{(\gamma-1)u^2}{2c^2} & \frac{(\gamma-1)u}{c^2} & -\frac{\gamma-1}{c^2} & \text{row}(\lambda_2)\\ \hline -\frac{u}{\rho}+\frac{(\gamma-1)u^2}{2\rho c} & \frac{1}{\rho}-\frac{(\gamma-1)u}{\rho c} & \frac{\gamma-1}{\rho c} & \text{row}(\lambda_3)\\ \hline \end{array} \tag{12}$$

with

$$\lambda_1=u-c \qquad \lambda_2=u \qquad \lambda_3=u+c \tag{13}$$

where $c=(\gamma p/\rho)^{1/2}$ is the speed of sound. The notation "row (λ_i)" denotes the row eigenvector corresponding to the eigenvalue λ_i.

At the inflow boundary,

$$L_1=\begin{bmatrix} & \vec{\ell}_1 & \\ \partial_\rho h & \partial_{\rho u} h & \partial_e h \\ \partial_\rho s & \partial_{\rho u} s & \partial_e s \end{bmatrix} \tag{14}$$

At the outflow boundary,

$$L_1=\begin{bmatrix} \partial_\rho p & \partial_{\rho u} p & \partial_e p \\ & \vec{\ell}_2 & \\ & \vec{\ell}_3 & \end{bmatrix} \tag{15}$$

The finite difference algorithm used may be written as[7,8]

$$\left\{I+(\Delta t)L_3^n\left[\delta_x A^n+\left(\frac{\partial \vec{H}}{\partial \vec{D}}\right)^n\right]+\epsilon_i\nabla_x\Delta_x\right\}(\vec{D}^{n+1}-\vec{D}^n)$$

$$=-(\Delta t)L_3^n(\delta_x\vec{E}^n+\vec{H}^n)-\epsilon_e[(\nabla_x\Delta_x)^2]\vec{D}^n \tag{16}$$

where ϵ_e and ϵ_i are the explicit and implicit smoothing coefficients, respectively.

$$\nabla_x\vec{D}=\vec{D}_{j+1}-\vec{D}_j \qquad \Delta_x\vec{D}=\vec{D}_j-\vec{D}_{j-1} \tag{17}$$

For interior points,

$$\delta_x=(\Delta_x+\nabla_x)/(2\Delta x) \text{ and } L_3=I$$

For boundary points

$$\delta_x=\nabla_x/(\Delta x) \text{ for inflow (left)}$$

$$\delta_x=\Delta_x/(\Delta x) \text{ for outflow (right)}$$

$$L_3=L_1^{-1}L_2$$

Numerical results are compared with the exact solution for this problem in Figs. 1a and 1b. The results were obtained for $y_{\min}=0.5$, $y_{\max}=0.75$, and for a CFL number of 25.0 using a 51-point grid.

$$\text{CFL number}=\frac{\Delta t}{\Delta x}(\text{maximum eigenvalue}|) \tag{18}$$

The close comparison between the numerical and exact solutions validates the numerical method.

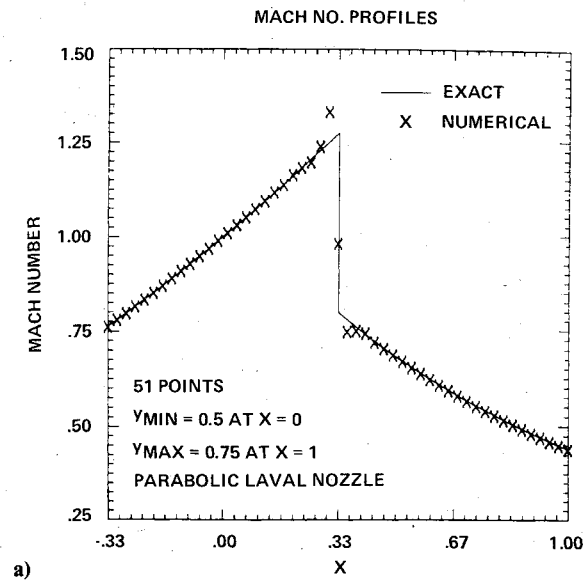

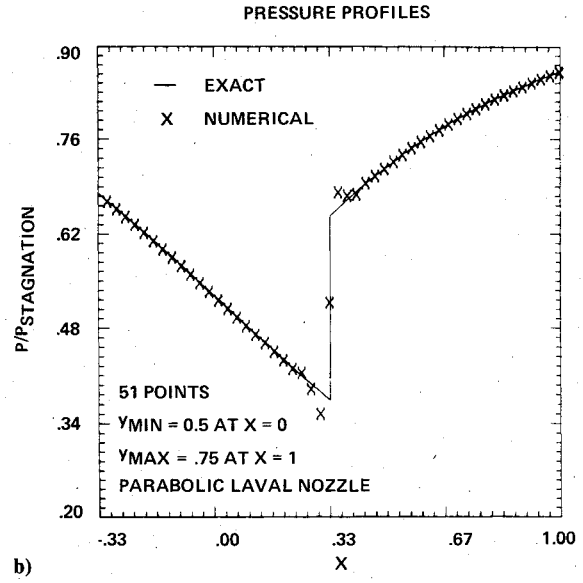

Fig. 1 a) Comparison of Mach number profiles for Laval nozzle flow. b) Comparison of pressure profiles for Laval nozzle flow.

Table 1 Computational CPU times for the example problems

CFL No.	Number of time steps	$\log_{10}$ (rms)	Computer time, CPU seconds
Laval nozzle flow, conservation law, 51 points, CDC 7600			
1.0	3000	−5	39.3
25.0	120	−5	1.33
Dual-throat nozzle flow, conservation law, $59\times14+43\times17$ points, Cyber 173			
1.0	2200	−2	1730.0
7.5	600	−4	460.0
Supersonic flow past sphere, SCM method, 21×21 points, CDC 7600			
1.0	800	−3 (variables), −2 (shock)	200.0
10.0	100	−3 (both)	25.0

Between every two time steps of the numerical solution process, the square of the change in each dependent variable was summed up. The square root of the average over all grid points of this sum was computed for each time step, normalized by its maximum value over all time steps and denoted by rms. Figure 2 displays the time history of $\log_{10}$ (rms) for two CFL numbers of 1.0 and 25.0. It is clear that while 3000 steps are required for decreasing the residue by five orders of magnitude using the smaller time step, the same convergence is attained after only 120 steps at a CFL number 25. A compilation of computer time required for this example and the others to follow is given in Table 1.

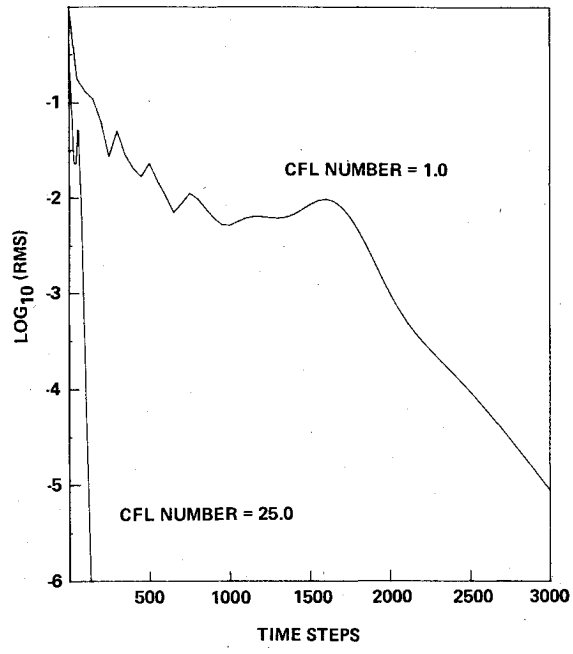

Fig. 2 Residue time history for Laval nozzle flow.

Two-Dimensional Theory

The theory and application of the implicit boundary point treatment presented for one spatial dimension are easily extended to more dimensions. Let the governing equation be written in the arbitrary coordinate system $\xi=\xi(x,y,t)$, $\eta=\eta(x,y,t)$, $\tau=t$ as

$$\hat{D}_\tau+\hat{E}_\xi+\hat{F}_\eta+\hat{H}=0 \tag{19}$$

where

$$\hat{D}=\vec{D}/J, \qquad \hat{E}=(\xi_t\vec{D}+\xi_x\vec{E}+\xi_y\vec{F})/J$$

$$\hat{F}=(\eta_t\vec{D}+\eta_x\vec{E}+\eta_y\vec{F})/J, \qquad \hat{H}=\vec{H}/J$$

and

$$\vec{D}=\begin{bmatrix}\rho\\ \rho u\\ \rho v\\ e\end{bmatrix} \qquad \vec{E}=\begin{bmatrix}\rho u\\ p+\rho u^2\\ \rho uv\\ (e+p)u\end{bmatrix}$$

$$\vec{F}=\begin{bmatrix}\rho v\\ \rho uv\\ p+\rho v^2\\ (e+p)v\end{bmatrix} \qquad \vec{H}=\frac{1}{y}\begin{bmatrix}\rho v\\ \rho uv\\ \rho v^2\\ (e+p)v\end{bmatrix}$$

$$J=\xi_x\eta_y-\eta_x\xi_y$$

$$=\text{Jacobian of transformation}$$

Equation (19) is in the conservation law form. Let

$$\hat{A}=\frac{\partial\hat{E}}{\partial\vec{D}} \qquad \hat{B}=\frac{\partial\hat{F}}{\partial\vec{D}} \qquad \hat{C}=\frac{\partial\hat{H}}{\partial\vec{D}} \tag{20}$$

The eigenvalues of $\hat{A}$ are (when scaled by the Jacobian J) given by

$$\lambda_1=\overline{U}-c\sqrt{\xi_x^2+\xi_y^2}, \qquad \lambda_{2,3}=\overline{U}, \qquad \lambda_4=\overline{U}+c\sqrt{\xi_x^2+\xi_y^2}$$

where

$$\overline{U}=\xi_t+u\xi_x+v\xi_y \tag{21}$$

and the eigenvalues of $\hat{B}$ are obtained from those of $\hat{A}$ by setting ξ to η. The left eigenvector matrix for $\hat{A}$ is given by

$$L=L_{\text{primitive}}M \tag{22}$$

where

$$L_{\text{primitive}}=\begin{array}{|cccc|l|}\hline 0 & -k_1 & -k_2 & 1/(\rho c) & \text{row }(\lambda_1)\\ c/\rho & k_2 & -k_1 & -1/(\rho c) & \text{row }(\lambda_2)\\ c/\rho & -k_2 & k_1 & -1/(\rho c) & \text{row }(\lambda_3)\\ 0 & k_1 & k_2 & 1/(\rho c) & \text{row }(\lambda_4)\\ \hline\end{array} \tag{23}$$

with

$$k_1=\xi_x/(\xi_x^2+\xi_y^2)^{1/2} \qquad k_2=\xi_y/(\xi_x^2+\xi_y^2)^{1/2}$$

and

$$M=\begin{array}{|cccc|}\hline 1 & 0 & 0 & 0\\ -u/\rho & 1/\rho & 0 & 0\\ -v/\rho & 0 & 1/\rho & 0\\ (\gamma-1)\dfrac{u^2+v^2}{2} & -(\gamma-1)u & -(\gamma-1)v & (\gamma-1)\\ \hline\end{array} \tag{24}$$

(see Ref. 9 or 10 for more details). The eigenvector matrix for $\hat{B}$ is again obtained from that for $\hat{A}$ by interchanging η for ξ in Eqs. (23) and (24).

With the above background information, the application of the boundary condition procedure is a straightforward extension of the theory for one spatial dimension. In fact, that theory is directly applied by partitioning off one of the two dimensions along with the source term conceptually into a composite source term. For boundaries where $\xi=$ constant, the η-derivative term is considered a source term; and for $\eta=$ constant boundaries, the ξ-derivative terms are grouped with $\hat{H}$ as a source term. The modified governing equations

that must be used at boundary points are thus simply

$$\hat{D}_\tau + L_1^{-1} L_2 (\hat{E}_\xi + \hat{F}_\eta + \hat{H}) = 0 \tag{25}$$

where the row eigenvectors are computed appropriately from either $\hat{A}$ or $\hat{B}$.

Then, the same approximately factored algorithm used at interior points may be applied to boundary points as follows:

$$\begin{aligned}
&[I + \Delta\tau J^{n+1} L_3^\eta (\delta_\xi \hat{A}^n + \hat{C}^n) + \epsilon_i \nabla_\xi \Delta_\xi] \\
&\times [I + \Delta\tau J^{n+1} (L_3^\eta \delta_\eta \hat{B}^n) + \epsilon_i \nabla_\eta \Delta_\eta] \cdot (\vec{D}^{n+1} - \vec{D}^n) \\
&= -\left(1 - \frac{J^{n+1}}{J^n}\right) \vec{D}^n - \Delta\tau J^{n+1} L_3^\eta (\hat{E}_\xi + \hat{F}_\eta + \hat{H})^n \\
&- \epsilon_e [(\nabla_\xi \Delta_\xi)^2 + (\nabla_\eta \Delta_\eta)^2] \vec{D}^n
\end{aligned} \tag{26}$$

with the previous definitions [see Eq. (17)] for L_3, δ_ξ, δ_η, etc., for interior and boundary points. It is interesting to note that L_3 multiplies all spatial and source terms and not just the derivative terms in the one coordinate direction for which L is defined.

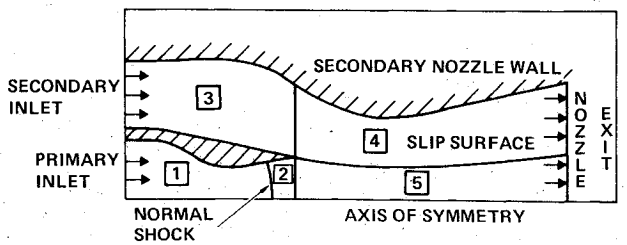

Fig. 3 Schematic diagram of mode 1 inviscid flow in dual-throat nozzle.

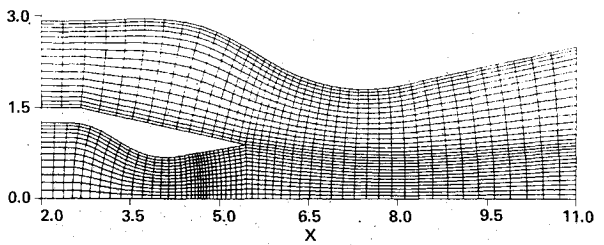

Fig. 4 Computational grid for implicit solution of conservation laws.

Dual-Throat Nozzle Flows

The two-dimensional theory of the last section is now applied to compute the inviscid flow through a dual-throat rocket engine nozzle. A schematic of such a nozzle is shown in Fig. 3. In the first mode of operation, both combustors (attached to the primary and secondary inlets) are in operation resulting in a normal shock in the primary nozzle and a slip line dividing the inner and outer streams. The conservation law form of the governing equations was solved on the grid of points shown in Fig. 4 using the implicit scheme given by Eq. (26).

The implicit boundary treatment for inflow and outflow have already been discussed for the Laval nozzle. A minor modification is made for two-dimensional flow to account for the extra repeated eigenvalue $\bar{U}$ and the extra dependent variable ρv. At inflow boundaries, now, three boundary conditions are needed. In addition to entropy and enthalpy, the vertical component of velocity is also specified (to be zero). Thus L_1 is made up of $\vec{\ell}_1$, $\partial h/\partial \vec{D}$, $\partial s/\partial \vec{D}$, $\partial v/\partial \vec{D}$. At the outflow, the specification of back pressure is sufficient for subsonic flow. To start the calculations, no flow and a low value of pressure are prescribed throughout the nozzle. The combustor (inlet) pressure (and thus enthalpy and entropy) are raised over a period of time towards their final steady values.[5] The outflow is subsonic to start with but eventually becomes supersonic. When this occurs, no boundary conditions are needed at the nozzle exit plane.

The application of surface tangency at the nozzle walls is now explained. Surface tangency is expressed as

$$\eta_x \rho u + \eta_y \rho v = 0 \tag{27a}$$

or in the time linearized fashion as

$$\eta_x (\rho u)_\tau + \eta_y (\rho v)_\tau = 0 \tag{27b}$$

At nozzle walls where only positive and zero eigenvalues account for propagation from interior to the nozzle wall,

$$L_1 = \begin{bmatrix} 0 & \eta_x & \eta_y & 0 \\ & \vec{\ell}_2 & & \\ & \vec{\ell}_3 & & \\ & \vec{\ell}_4 & & \end{bmatrix} \tag{28}$$

and the first row of L_2 is zero. The matrices L_1 and L_2 for nozzle walls where positive eigenvalues must be discarded are similarly derived.

Mach number and pressure contours obtained from this implicit method are shown in Figs. 5a and 5b and the results are compared with results from another numerical method in Figs. 5c-5e. This second method, labeled the SCM (split coefficient matrix) method in the plots, employs "fitting" procedures to treat the shock wave and slip line as precise discontinuities. For more details on the application of the SCM method[4] to dual-throat nozzle flows, the reader is referred to Ref. 5. The close comparison of the results obtained using these two independently derived methods validates both methods. In these results, zones 1 and 2 denote the regions below and above the slip line, respectively.

A time history of $\log_{10}$ (rms) for this example problem is displayed in Fig. 6 for two CFL numbers 1.0 and 7.5. For the first case, the combustor pressures reached final steady-state values [p_0(inner) = 1.0, p_0(outer) = 0.925] after 500 steps. For the second case (CFL number of 7.5), the transient pressure rise was imposed over 200 steps. The dramatic increase in convergence rate is clearly seen for the larger time step. About four orders of magnitude reduction in the rms value takes but 400 steps after complete combustor pressure rise. The solution converges very slowly for the smaller time step.

Shock Fitting

The last example is the supersonic flow past a sphere. A bow shock stands upstream of the sphere and the objective is to implicitly "fit" this shock as a computational boundary.

Let the shock be defined by $\eta = \eta_{\max}$. At a shock point only the fourth eigenvalue

$$\lambda_4 = \eta_t + u\eta_x + v\eta_y + c\sqrt{\eta_x^2 + \eta_y^2}$$

is positive and accounts for signal propagation from the interior of the domain to the boundary. Upstream of the shock, the dependent variables take on their freestream values. Downstream of the shock, if pressure (for convenience) is known, then the Rankine-Hugoniot jump relations provide enough equations to compute density, the velocity components and the shock speed (normal to itself). Thus, at a shock point, one may construct derivatives $\partial\rho/\partial p$, $\partial u/\partial p$, $\partial v/\partial p$ from the Rankine-Hugoniot relations (see any text on gasdynamics or Ref. 4). From these $\partial \vec{D}/\partial p$ may also

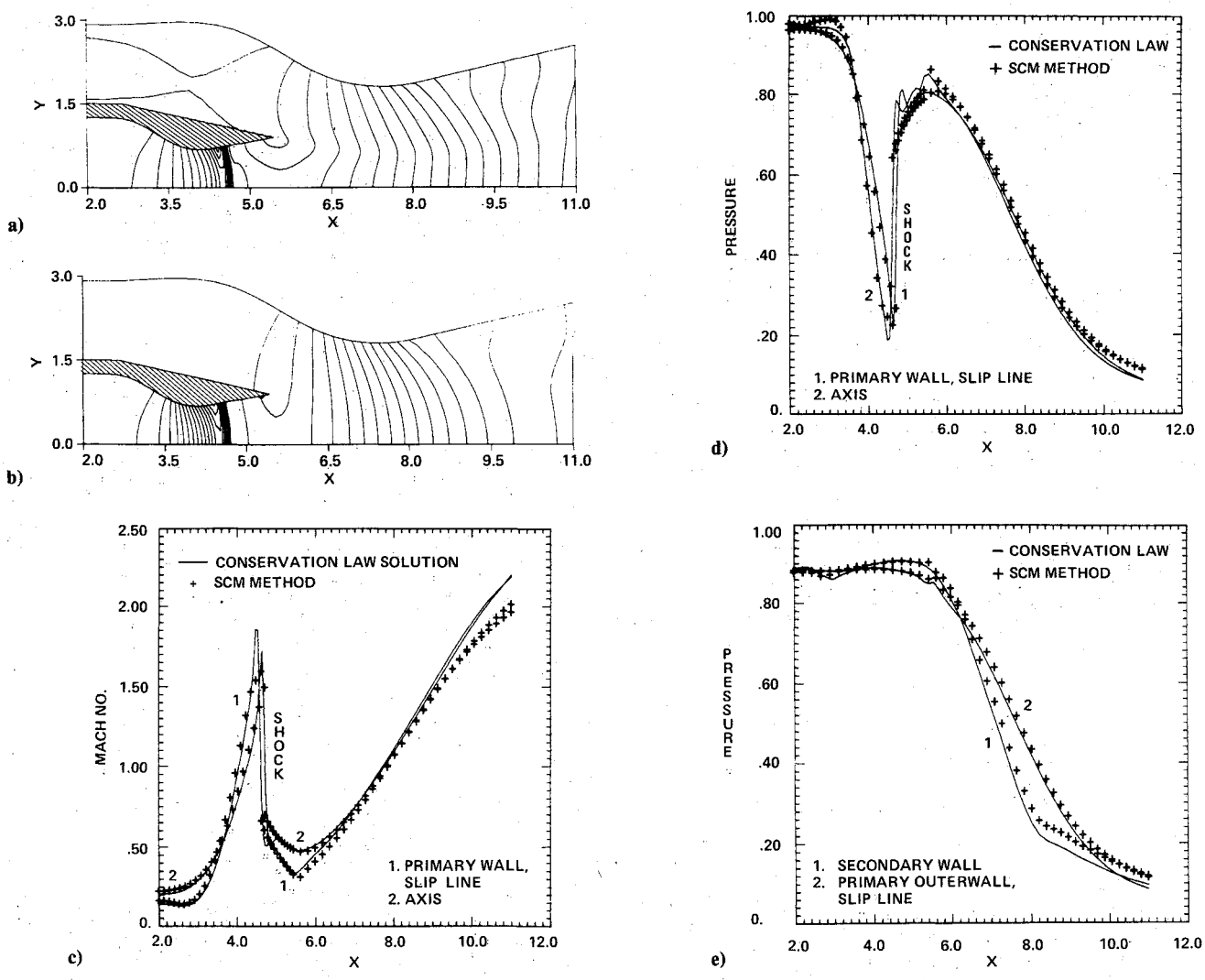

Fig. 5 a) Mach number contours in dual-throat rocket nozzle. b) Pressure contours in dual-throat rocket nozzle. c) Mach number profiles in zone 1: SCM vs conservation law. d) Pressure profiles in zone 1: SCM vs convention law. e) Pressure profiles in zone 2: SCM vs conservation law.

be constructed. With this background, a minor modification of the implicit boundary procedures presented in the earlier sections yields the equations to be solved implicitly at the shock.

The one compatibility equation valid at the shock is

$$\vec{\ell}_4(\hat{D}_\tau + \hat{E}_\xi + \hat{F}_\eta + \hat{H}) = 0 \tag{29a}$$

or

$$\vec{\ell}_4 \frac{\partial \hat{D}}{\partial p} p_\tau + \vec{\ell}_4(\hat{E}_\xi + \hat{F}_\eta + \hat{H}) = 0 \tag{29b}$$

Denoting the product $\vec{\ell}_4(\partial\hat{D}/\partial p)$ by N, Eq. (29b) may be rewritten as

$$p_\tau = -\frac{1}{N}\vec{\ell}_4(\hat{E}_\xi + \hat{F}_\eta + \hat{H}) = 0 \tag{29c}$$

Since $\hat{D}_\tau = (\partial\hat{D}/\partial p)p_\tau$, we have

$$\hat{D}_\tau + \frac{1}{N}\frac{\partial \hat{D}}{\partial p}\vec{\ell}_4(\hat{E}_\xi + \hat{F}_\eta + \hat{H}) = 0 \tag{30}$$

which may be transcribed into the familiar form

$$\hat{D}_\tau + L_I^{-1} L_2(\hat{E}_\xi + \hat{F}_\eta + \hat{H}) = 0$$

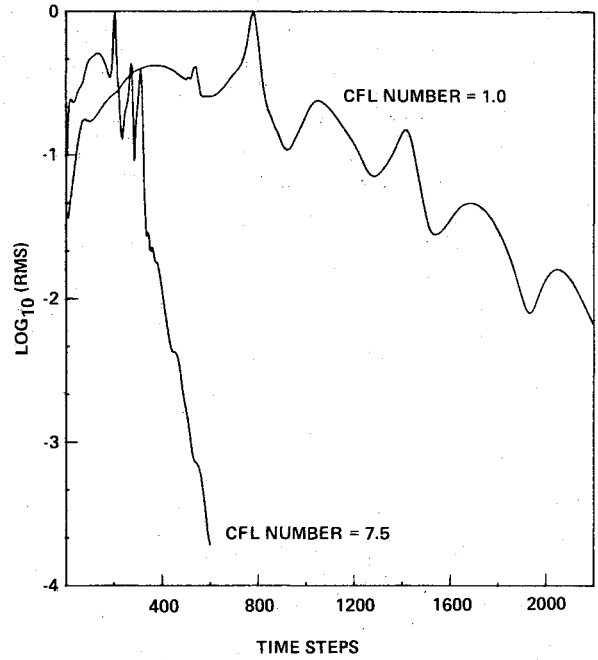

Fig. 6 Time history of rms change in dependent variables for dual-throat nozzle flow.

where

$$L_1^{-1}L_2 = \frac{1}{N}\begin{bmatrix} \partial_p d_1 \vec{\ell}_4 \\ \partial_p d_2 \vec{\ell}_4 \\ \partial_p d_3 \vec{\ell}_4 \\ \partial_p d_4 \vec{\ell}_4 \end{bmatrix} \tag{31}$$

(The elements of $\hat{D}$ have been denoted by d_i.)

To start the calculations, the shock shape and speed are chosen (speed is usually set to zero). The solution behind the shock is known from Rankine-Hugoniot relations. The rest of the flowfield is also initialized approximately. The implicit scheme [Eq. (26)] is applied in one step including Eq. (31) at the shock to update the dependent variables. The new pressure behind the shock is used to calculate the new shock velocity which in turn is used to move the grid and define grid point velocities for the next step.

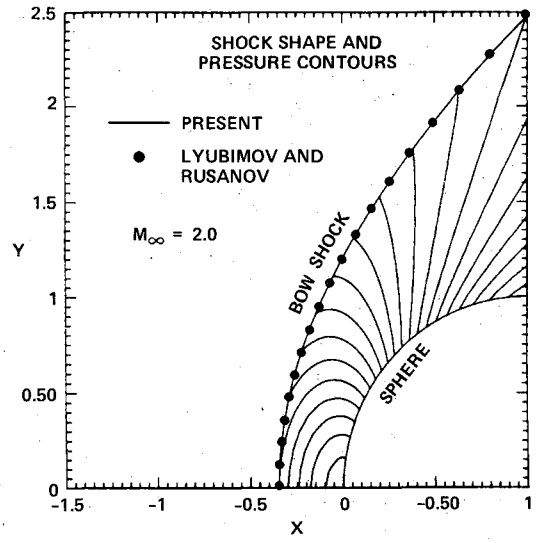

a)

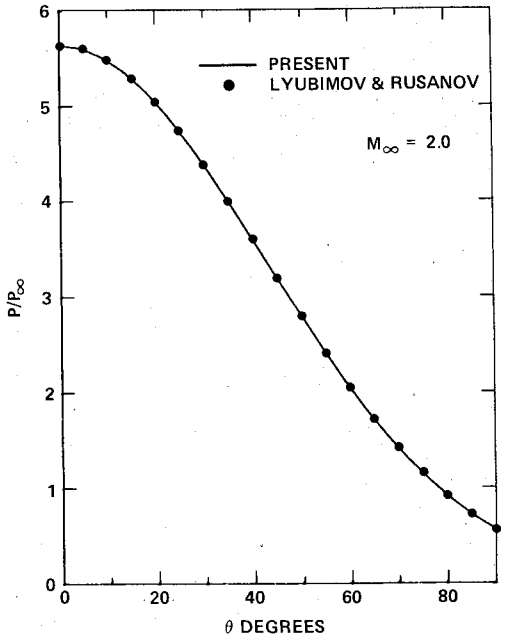

b)

Fig. 7 a) Comparison of shock location for supersonic flow past a sphere. b) Comparison of surface pressure distribution for supersonic flow past a sphere.

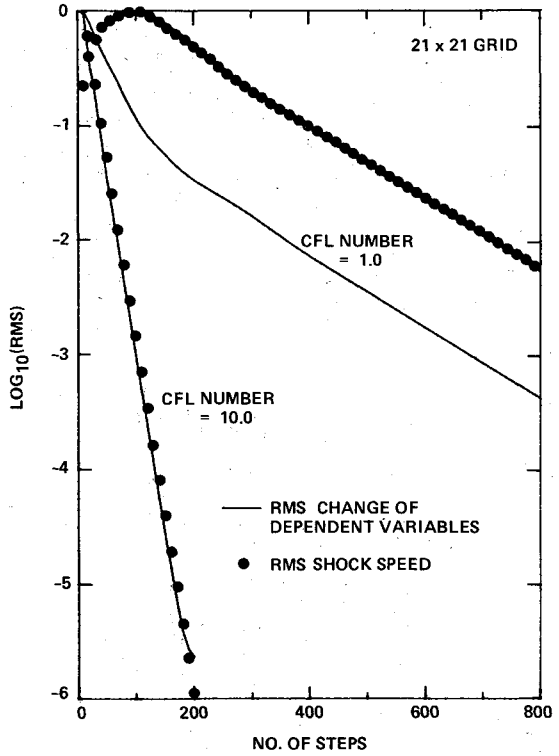

Fig. 8 Time history of rms change in dependent variables and rms shock speed for supersonic flow past blunt body with shock "fitting."

The results that follow used the SCM method applied to the nonconservation form of the equations

$$\vec{D}_\tau + \hat{A}\vec{D}_\xi + \hat{B}\vec{D}_\eta + \vec{H} = 0 \tag{32}$$

with

$$\vec{D} = \begin{bmatrix} \ell n(p/\rho^\gamma) \\ u \\ v \\ \ell n(p) \end{bmatrix}$$

and consequently different choices for $\hat{A}$, $\hat{B}$, and $\hat{H}$ than for the conservation dependent variables used earlier. Thus the implicit procedure at boundaries is given by a two-dimensional extension of Eq. (7c):

$$\vec{D}_\tau + L_1^{-1}L_2(\hat{A}\vec{D}_\xi + \hat{B}\vec{D}_\eta + \hat{H}) = 0 \tag{33}$$

Similar results have also been obtained using the conservation form.

Numerical results obtained using the method under consideration are compared with results from Lyubimov and Rusanov[11] in Figs. 7a and 7b. The two solutions match almost exactly for this case with $M_\infty = 2.0$. The implicit scheme used a grid of 21×21 points. The time history of the $\log_{10}$ (rms) is shown in Fig. 8 for two CFL numbers 1.0 and 10.0. The advantage of using a larger time step is obvious. Six orders of magnitude reduction in both shock speed and flowfield change take less than 200 steps with CFL number 10.0. For an accuracy comparable to 800 steps with CFL number 1.0, it takes but 50 steps at the larger time step.

Concluding Remarks

New, implicit boundary condition procedures have been described for use with implicit finite difference methods.

When boundary points are treated explicitly, even though interior points may be solved by implicit schemes, a CFL number of 1.0 will be the maximum possible for stability. The implicit boundary treatment presented avoids such restrictions. The increase in computational speed made possible by the new method is clearly seen when results for a larger CFL number are compared with results for a CFL number of unity. At least an order of magnitude speed up has been shown for the examples presented. These examples have also been used to show detailed application of the new methodology to specific types of boundaries. Subsonic inflow and outflow were introduced in the discussion of quasi-one-dimensional Laval nozzle flow. Surface tangency was covered along with dual-throat nozzle flows and shock fitting described in conjunction with supersonic flows past bluff bodies.

The new method is applicable to both the conservation and the nonconservation law form. It is obvious that the discrete analog of the conservation property is not strictly satisfied at boundaries. This is only partly a result of modifying the spatial derivatives and source term with $L_I^{-1}L_2$. It is also because, usually, the finite difference approximation used at the boundary point is not consistent with that used at interior points from the point of view of obtaining global conservation. In fact, when

$$\delta_x f = \frac{f_{j+1} - f_{j-1}}{2\Delta x} \tag{34}$$

for interior points, at the left boundary, the operator must be defined to be

$$\delta_x f = \frac{f_{j+1} - f_j}{2\Delta x} \tag{35}$$

for global conservation. It will be interesting to try Eq. (35) in future test problems.

In the new methodology presented, only time-linearized boundary conditions are utilized. Therefore, for nonlinear boundary conditions, the solution at the updated or new time level would only be satisfied approximately. Approximate factorization procedures for multidimensional problems introduce other errors. Consequently, after the solution is advanced one step, the independent variables at boundary points must be overwritten to satisfy the boundary conditions exactly. Another approach would be to reformulate the boundary conditions so that they help drive the residual in satisfying the boundary condition to zero:

$$\frac{\partial B_i^n}{\partial \vec{D}} (\vec{D}^{n+1} - \vec{D}^n) = -B_i^n \tag{36}$$

and not worry about overwriting dependent variables. This latter approach has not been utilized in the results presented above.

References

[1] Kentzer, C.P., "Discretization of Boundary Conditions on Moving Discontinuities," in *Lecture Notes in Physics,* No. 8, Springer-Verlag, N.Y.; see also *Proceedings of the Second International Conference on Numerical Methods in Fluid Dynamics,* Berkeley, Calif., Sept. 15-19, 1970, pp. 108-113.

[2] Porter, R.W. and Coakley, J.F., "Use of Characteristics for Boundaries in Time Dependent Finite Difference Analysis of Multidimensional Gas Dynamics," *International Journal for Numerical Methods in Engineering,* Vol. 5, 1972, pp. 91-101.

[3] deNeef, T., "Treatment of Boundaries in Unsteady Inviscid Flow Computations," Delft University of Technology, Delft, The Netherlands, Department of Aerospace Engineering Report LR-262, Feb. 1978.

[4] Chakravarthy, S.R., Anderson, D.A., and Salas, M.D., "The Split-Coefficient Matrix Method for Hyperbolic Systems of Gasdynamic Equations," AIAA Paper 80-0268, Jan. 1980.

[5] Chakravarthy, S.R., "Inviscid Analysis of Dual-Throat Nozzle Flows," AIAA Paper 81-1201, June 1981.

[6] Whitham, G.B., *Linear and Nonlinear Waves,* John Wiley and Sons, New York, 1974.

[7] Beam, R.M. and Warming, R.F., "An Implicit Factored Scheme for the Compressible Navier-Stokes Equations," *Proceedings of the AIAA 3rd Computational Fluid Dynamics Conference,* Albuquerque, N.M., June 27-28, 1977, pp. 130-140.

[8] Steger, J.L., "Implicit Finite-Difference Simulation of Flow about Arbitrary Two-Dimensional Geometries," *AIAA Journal,* Vol. 16, July 1978, pp. 679-686.

[9] Chakravarthy, S.R., "The Split-Coefficient Matrix Method for Hyperbolic Systems of Gasdynamic Equations," Ph.D. Thesis, Dept. of Aerospace Engineering, Iowa State Univ., Ames, Iowa, Nov. 1979.

[10] Warming, R.F., Beam, R.M., and Hyett, B.J., "Diagonalization and Simultaneous Symmetrization of the Gasdynamic Matrices," *Mathematics of Computation,* Vol. 29, Oct. 1975, pp. 1037-1045.

[11] Lyubimov, A.N. and Rusanov, V.V., "Gas Flows Past Blunt Bodies," NASA TT-F 715, Feb. 1973.